Observables in high-statistics measurements of the reaction $\bar{p}p \to \bar{\Lambda}\Lambda$

P. D. Barnes, G. Diebold, G. Franklin, B. Quinn, R. Schumacher, J. Seydoux, and V. Zeps
Carnegie-Mellon University, Pittsburgh, Pennsylvania 15260

P. Birien, W. Dutty, H. Fischer, J. Franz, E. Rössle, H. Schledermann, H. Schmitt, and R. Todenhagen
Universität Freiburg, Freiburg, Germany

W. Breunlich and N. Nägele
Institut für Mittelenergiephysik der ÖAW, Vienna, Austria

R. Bröders, R. v. Frankenberg, K. Kilian, W. Oelert, K. Röhrich, K. Sachs, T. Sefzick, G. Sehl, and M. Ziolkowski
Institut für Kernphysik der KFA Jülich, Jülich, Germany

R. A. Eisenstein, D. Hertzog, and R. Tayloe
University of Illinois, Urbana, Illinois 61801

H. Dennert, W. Eyrich, R. Geyer, J. Hauffe, A. Hofmann,* M. Kirsch, R. A. Kraft, and F. Stinzing
Universität Erlangen-Nürnberg, Nürnberg, Germany

N. Hamann*
CERN, Geneva, Switzerland

T. Johansson and S. Ohlsson
Uppsala University, Uppsala, Sweden
(Received 6 February 1996)

Associated strangeness production has been studied in the $\bar{p}p \to \bar{\Lambda}\Lambda \to \bar{p}\pi^+ p\pi^-$ reaction at the CERN antiproton facility LEAR using the experimental setup of PS185. Results from two high-statistics measurements at incident antiproton momenta of 1.642 and 1.918 GeV/c are reported. Approximately 40 000 reconstructed events at each momentum have allowed us to measure the total and differential cross sections, the spin polarizations, the spin correlations, and the singlet fractions of the $\Lambda\bar{\Lambda}$ pair. Since the decays of both the Λ and the $\bar{\Lambda}$ were simultaneously observed in the same detector, we are able to provide upper limits on CP and CPT violation phenomena in the weak interaction. [S0556-2813(96)03910-6]

PACS number(s): 25.43.+t, 11.30.Er, 13.75.Cs, 14.20.Jn

I. INTRODUCTION

In a systematic study over several years [1–7] the PS185 collaboration at the Low-Energy Antiproton Ring at CERN (LEAR/CERN) has been investigating antihyperon-hyperon ($\bar{Y}Y$) production and decay via the reaction $\bar{p}p \to \bar{Y}Y$. The focus of this work is to explore the physics of strange quark production and the role of the s quark in the configuration of the emerging hyperons. Our experiments build on several earlier studies [8–12] that used incident momenta ranging from 1.5 to 6 GeV/c. The principal advantages of the recent PS185 studies lie in their momentum resolution and consequent ability to approach the reaction threshold very closely, their generally high statistics, and the measurement of an almost complete set of spin observables. The high quality of the resulting data set is due in large measure to the extraordinary qualities of the LEAR/CERN accelerator complex.

Our studies, involving production of the Λ and Σ hyperons, have taken place at several incident momenta, ranging from the threshold for $\bar{\Lambda}\Lambda$ production (1.4356 GeV/c), to momenta close to the upper limit of the LEAR facility (2.0 GeV/c). For $\bar{\Lambda}\Lambda$ production, the latter value corresponds to an excess kinetic energy ($\epsilon = \sqrt{s} - m_{\bar{\Lambda}} - m_{\Lambda}$) of 199 MeV. We have measured precise values for the total and differential cross sections at each incident momentum. In most cases (excepting those closest to threshold) we have also been able to measure the spin polarizations and correlations of the outgoing hyperons. It is hoped that this additional information about the basic amplitudes will be of significant help in constraining theoretical models of strange quark production.

At each momentum studied, the crucial role played by strong annihilation in $\bar{p}p$ reactions is readily apparent. Indeed, the reaction cross sections for the two-body hyperon final states are very small compared to those for annihilation into pionic final states. For example, the total cross section for $\bar{\Lambda}\Lambda$ production is observed to rise steeply from threshold to excess energies around 50 MeV ($p_{\bar{p}} \sim 1.6$ GeV/c) as phase space increases, followed by a slow increase from 60 μb to about 100 μb at 2 GeV/c. This value is about 1000 times smaller than what is observed for pion production.

*Deceased.

Similarly, our measured differential cross sections and polarizations [1–5] display features that are characteristic of strong interaction dynamics [13,14]. These matters are discussed further below.

In the lower-momentum range, PS185 data very close to threshold have been published [3,5]. Data taking has recently been extended in that region to explore an unexpected structure in the total cross section behavior at $\epsilon \sim 1$ MeV excitation energy [5]. In the intermediate- and higher-momentum range, additional data are presently being analyzed (Bröders [1], Dennert [1], Sachs [1], and Tayloe [1]).

The reaction dynamics of the $\bar{p}p \rightarrow \bar{\Lambda}\Lambda$ transition have been studied in many theoretical papers [15–42]. These descriptions have been of three general types: (1) the strangeness production originates from the t-channel exchange of K mesons [15–21]; (2) the process originates from the s-channel annihilation of a $\bar{u}u$ pair and the subsequent production of an $\bar{s}s$ pair that is accompanied by four ''spectator'' quarks [22–32] (other work has focused on quark descriptions via quark counting rules [33]), and (3) model-independent analyses of the low-momentum data that are based on a partial-wave amplitude decomposition [34–36]. Since only a few partial waves contribute here, it may be possible to learn more about the underlying reaction mechanism. Additional work [37–39] has also been done in the threshold region to study the possible anomaly [5] in the total cross section data mentioned above.

The typical collision distances are expected to be short due to the large momentum transfer necessary to create the final state hyperons. This leads to the expectation that quark effects might be important, even though K-meson exchanges describe the experimental data very well. However, given the strongly absorbing nature of these reactions, we expect that initial- and final-state interactions will be of major significance, and may, barring a deeper understanding of absorptive processes, cloud our ability to learn more about the detailed nature of the production process. In order to deal with a mixture of strongly coupled and weakly coupled channels acting in the same problem, coupled-channel techniques have been used [40–42] to interpret the data.

In this paper we present two high-statistics measurements of the $\bar{p}p \rightarrow \bar{\Lambda}\Lambda \rightarrow \bar{p}\pi^+ p\pi^-$ process. The data set at 1.642 GeV/c incident $\bar{p}$ momentum lies just below the opening of the $\bar{p}p \rightarrow \bar{\Lambda}\Sigma^0 +$c.c. channel. The other set, taken at 1.918 GeV/c, lies above the thresholds for the $\bar{p}p \rightarrow \bar{\Sigma}^{\pm}\Sigma^{\pm}$ channels. Measured values for the $\bar{\Lambda}\Sigma^0 +$c.c. (Tayloe [1]) and $\bar{\Sigma}^{\pm}\Sigma^{\pm}$ (Geyer [1]) cross sections at these momenta will be presented in a forthcoming publication. They will augment the earlier $\bar{\Lambda}\Sigma^0 +$c.c. data [6] published by PS185.

II. DETECTION AND DATA ANALYSIS

A. Detector

The PS185 experiment is designed for high-acceptance measurements of the $\bar{p}p \rightarrow \bar{\Lambda}\Lambda$ reaction from very near threshold to 2 GeV/c over the entire 4π solid angle. The charged weak decay mode $\bar{p}p \rightarrow \bar{\Lambda}\Lambda \rightarrow \bar{p}\pi^+ p\pi^-$ provides the signature that is used to determine events by kinematic fitting. It also permits a statistical determination of the final-state spin observables [43]. The experimental setup, shown in Fig. 1, is described in detail in [1–4]. It is designed around a nonmagnetic decay spectrometer consisting of a segmented target neutral trigger system, a set of MWPC and MWDC tracking detectors, a fast scintillation detector (trigger) hodoscope, and a ''baryon identifier.'' The latter consists of a 0.09 T magnetic solenoid that incorporates three drift chamber planes that are used to distinguish hyperons from antihyperon vertices.

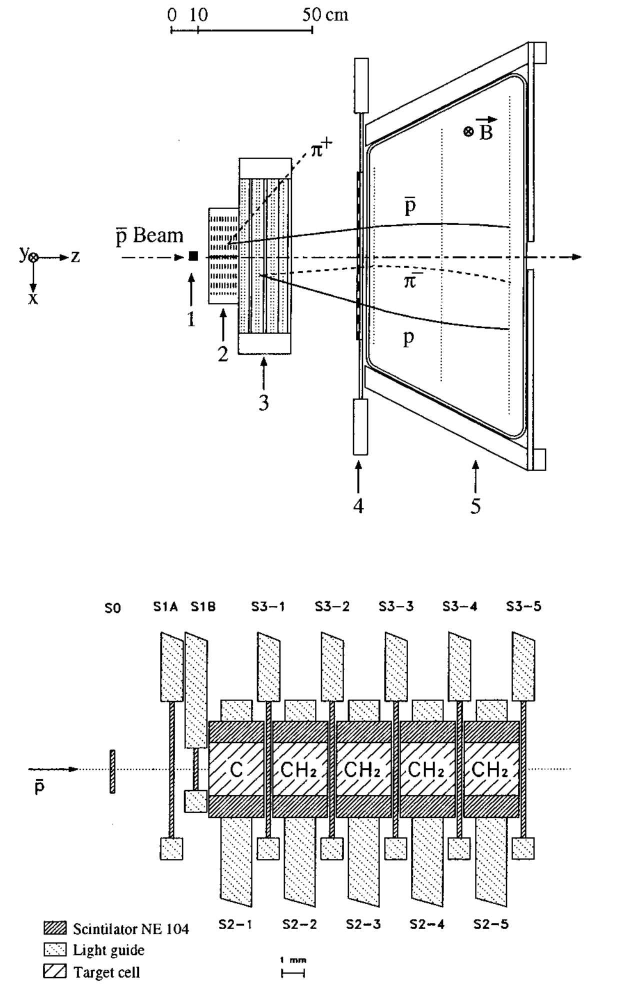

FIG. 1. Overview of the PS185 detector system. (1) segmented neutral trigger target, (2) multiwire proportional chambers (MWPC's), (3) multiwire drift chambers (MWDC's), (4) scintillator hodoscope, and (5) solenoid ''baryon indentifier'' with drift chambers. The lower part of the figure shows a detail of the segmented target.

For the data reported here, the target consisted of several small individual CH_2 elements, each having a diameter of 2.5 mm and a length of 2.5 mm. Either three or four target elements were used, depending on the conditions desired for the run in question. Each target element was ''sandwiched'' between, and surrounded by, an array of small scintillators in order to provide precise information about the incident momentum and the position of the reaction point, as well as a signature for the neutral-particle final state. A pure ^{12}C target cell allowed study of background events arising from carbon in the CH_2 target.

B. Data analysis

The analysis is based on reconstructing events with two V's from the delayed decays of a $\bar{\Lambda}\Lambda$ pair. The decays lead to the charged particle pairs $\bar{p}\pi^+$ and $p\pi^-$, respectively. Two-dimensional tracks are fitted to hits in the MWPC and MWDC planes and then matched between the two detectors to form three-dimensional tracks. Candidate V's are constructed from two three-dimensional tracks that intersect at a point downstream from the target and which are sufficiently coplanar with the interaction point. Candidate two-V events are formed if there are two V's with vertices consistent with two-body kinematics. A full kinematic fit is performed to determine if the data agree with the $\bar{p}p \to \bar{\Lambda}\Lambda \to \bar{p}\pi^+ p\pi^-$ hypothesis. Each V is assigned to a Λ or a $\bar{\Lambda}$ based on the sagitta of the decay tracks in the magnetic field of the ''baryon identifier.'' Because we have a kinematically overconstrained situation, we are able to obtain a $\Lambda\bar{\Lambda}$ sample that is quite free of background.

III. EVALUATION OF THE CROSS SECTION

In order to evaluate the total and differential cross sections, several corrections had to be performed on the data. These are described briefly below. Fuller accounts may be found in Refs. [1–7].

(1) Since each $\bar{p}$ in the beam is registered individually, a correction is made for approximately 0.7% loss of beam flux in each target cell, due to nuclear interactions other than the channel of interest, and for straggling. In addition, the knockout of δ electrons causes a trigger inefficiency, requiring a correction of approximately 5% for a CH_2 cell and 2% for a ^{12}C cell. These numbers are calculated estimates and are about the same for the two momenta 1.642 and 1.918 GeV/c.

(2) There is also a correction arising due to $\bar{p}p \to \bar{\Lambda}\Lambda$ reactions from protons bound in the ^{12}C of the CH_2 cells. It is determined by reconstructing events from the special carbon cell that was installed for this purpose. This background was of order (5–10)% and was determined with statistical errors of 10% or better. It was subtracted for each angular bin individually at each momentum value.

(3) Corrections due to uncertainties in track fitting were addressed using a χ^2 criterion. The kinematic fitting procedure used generally required that $\chi^2 \leqslant 5$. Since that value is somewhat arbitrary, a Monte Carlo simulation was used to determine an appropriate correction at each momentum setting. The values of this correction were $(5.7\pm1.0)\%$ at 1.642 GeV/c and $(6.5\pm1.1)\%$ at 1.918 GeV/c. A Monte Carlo procedure was necessary because the errors are non-Gaussian in nature.

(4) Corrections in the range of $(1.6\pm0.8)\%$, due to possible reactions of the decay particles in the detector material, were made using known reaction cross sections and detector density distributions.

(5) Corrections due to the experimental acceptance, which range from 56% for forward or backward production to 29% at center-of-mass production angles of 90°, included effects from on-line triggering, reconstruction efficiency, and baryon number identification. These were calculated from Monte Carlo simulations of the experiment using 389 142 and 350 000 generated events at 1.642 and at 1.918 GeV/c, respectively.

(6) Finally, the branching ratio for charged particle decay of the $\bar{\Lambda}\Lambda$ pair was taken into account by using the factor $(0.641\pm0.005)^2$ [44].

IV. SPIN OBSERVABLES

Spin observables are a crucial part of the physics we want to study in the $\bar{p}p \to \bar{\Lambda}\Lambda$ reaction. The density matrix formalism in the helicity basis [14,16,45] is a particularly clear and elegant way to follow the development of the spin states as the reaction progresses.

It is well known that the density matrix ρ, for a collection of *uncorrelated* spin-$\frac{1}{2}$ particles, can be written as $\rho = \frac{1}{2}(I+\vec{\sigma}\cdot\vec{P})$, where I is the 2×2 unit matrix, $\vec{\sigma}$ are the Pauli spin matrices, and $\vec{P}$ is the average spin polarization vector of the sample. Because the initial antiproton beam and the hydrogen target each consists of spin-$\frac{1}{2}$ particles which are assumed to be uncorrelated, the spins in the initial $\bar{p}p$ system can be represented by the following outer product of 2×2 density matrices:

$$\rho_{\bar{p}p} = \tfrac{1}{2}(I+\vec{\sigma}\cdot\vec{P})_{\bar{p}} \otimes \tfrac{1}{2}(I+\vec{\sigma}\cdot\vec{P})_{p}. \tag{1}$$

So by construction $\rho_{\bar{p}p}$ is a separable 4×4 matrix in $\bar{p}p$ spin space. When the initial polarizations are zero, the $\bar{p}p$ density matrix is $\frac{1}{4}I$, where I is the unit matrix in 4×4 space.

To obtain the final-state density matrix $\rho_{\bar{\Lambda}\Lambda}$ from $\rho_{\bar{p}p}$, we operate with the strong interaction transition matrix T as follows:

$$\rho_{\bar{\Lambda}\Lambda} = T(\theta_{\bar{\Lambda}})\rho_{\bar{p}p}T^{\dagger}(\theta_{\bar{\Lambda}}). \tag{2}$$

Here θ is the scattering angle in the center-of-momentum frame. Since the final state consists of spin-$\frac{1}{2}$ particles, the $\bar{p}p \to \bar{\Lambda}\Lambda$ T matrices will also be 4×4. All of the physics of the transition is contained in the $T(\theta)$ matrices, and it is here that models of the underlying process can be used to make predictions to compare with experiment. In general, after the transition indicated by Eq. (2), the resulting density matrix will no longer be separable.

As usual in the density matrix formalism, the observables of the experiment are calculated by taking the trace of the product of the density matrix and the matrix representing the operator of interest. For example, in the $\bar{p}p \to \bar{\Lambda}\Lambda$ case we have for the differential cross section $d\sigma/d\Omega = (\mathrm{tr}\rho_{\bar{\Lambda}\Lambda}/\mathrm{tr}\rho_{\bar{p}p})$ and for the spin observables

$$P_{\bar{y}} = \frac{\mathrm{tr}(\rho_{\bar{\Lambda}\Lambda}\cdot\sigma_{\bar{y}}\otimes I_{\Lambda})}{\mathrm{tr}\rho_{\bar{\Lambda}\Lambda}}, \tag{3}$$

$$C_{\bar{m}n} = \frac{\mathrm{tr}(\rho_{\bar{\Lambda}\Lambda}\cdot\sigma_{\bar{m}}\otimes\sigma_{n})}{\mathrm{tr}\rho_{\bar{\Lambda}\Lambda}}, \quad \text{etc.} \tag{4}$$

Here $\hat{y}$ is the direction perpendicular to the reaction plane, $\hat{y} = \vec{p}_{\bar{p}} \times \vec{p}_{\bar{\Lambda}} / |\vec{p}_{\bar{p}} \times \vec{p}_{\bar{\Lambda}}|$, and we denote the $\bar{\Lambda}$ polarization in the $\hat{y}$ direction using the notation $P_{\bar{y}}$.

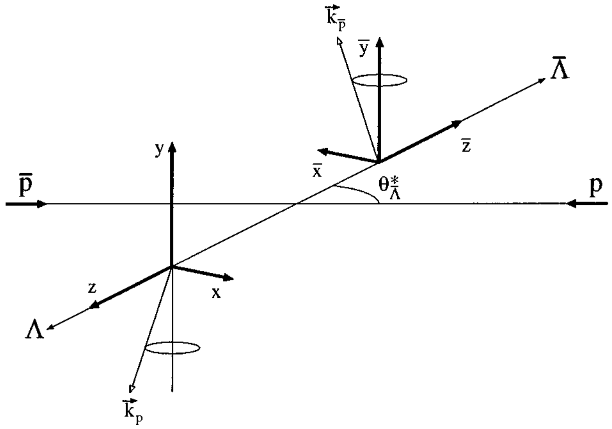

FIG. 2. Definition of the coordinates in the $\bar{p}p$ and $\bar{\Lambda}\Lambda$ center-of-momentum system and in the $\bar{\Lambda}$ and Λ rest frames.

The final-state $\bar{\Lambda}\Lambda$ density matrix $\rho_{\bar{\Lambda}\Lambda}$ can be expressed in terms of any complete set of 4×4 matrices. Fortunately, in the spin-$\frac{1}{2}$ on spin-$\frac{1}{2}$ case, this set of matrices can be chosen [16] to be the matrices corresponding to the usually observed experimental quantities of interest, viz.,

$$\rho_{\bar{\Lambda}\Lambda}=\tfrac{1}{4}\mathcal{I}(\theta_{\bar{\Lambda}})\Bigg[I_{\bar{\Lambda}}\otimes I_{\Lambda}+\vec{\sigma}\cdot\vec{P}_{\bar{\Lambda}}\otimes I_{\Lambda}+I_{\bar{\Lambda}}\otimes\vec{\sigma}\cdot\vec{P}_{\Lambda}+\sum_{mn}C_{\bar{m}n}\sigma_{\bar{m}}\otimes\sigma_n\Bigg]. \tag{5}$$

Here the $C_{\bar{m}n}$ are the spin correlation coefficients of the $\bar{\Lambda}\Lambda$ pair, with the $(\bar{m},n)$ indices denoting the axes of the $\bar{\Lambda}\Lambda$ rest mass coordinate system as defined in Fig. 2. The quantity $\mathcal{I}(\theta)$ is proportional to the differential cross section.

Because of the self-analyzing weak decay of the Λ hyperon [43] and the high intensity of the LEAR beam, all of these quantities are experimentally observable in PS185 in a statistically significant sample and therefore the spin situation in the exit hyperon channel is known. The angular distribution of the weak decay products can be obtained by calculating the density matrix for the final state [16] using the T matrices for the weak decays:

$$\rho_{\bar{p}\pi^+;p\pi^-}=T_w\rho_{\bar{\Lambda}\Lambda}T_w^{\dagger}. \tag{6}$$

Since each Λ and $\bar{\Lambda}$ decay is independent, T_w is an outer product of 2×2 matrices, one for each particle [16].

The two different present-day dynamical approaches, the s-channel quark-gluon model and the t-channel K-exchange process, are equally successful at describing the experiments. There seems to be little in the present data to distinguish between them, especially with respect to the cross section information. However, the polarization and spin correlation measurements of the final-state $\bar{\Lambda}\Lambda$ hyperons are much more sensitive to model input, and so we look to them for ways to distinguish between calculations. As outlined above, these quantities are quantum-mechanical expectation values of operators constructed from the Pauli matrices, e.g.,

$$\vec{P}_{\bar{\Lambda}}=\langle\vec{\sigma}_{\bar{\Lambda}}\otimes I_{\Lambda}\rangle \quad \text{and} \quad C_{\bar{m}n}=\langle\sigma_{\bar{m}}\otimes\sigma_n\rangle. \tag{7}$$

The number of independent spin observables is reduced substantially because of parity (P) conservation and charge conjugation (C) symmetry. Parity requires that all components of polarization *induced by the strong interaction, and lying in the reaction plane,* must vanish. That is, for an unpolarized initial state, we have $P_x=P_z=P_{\bar{x}}=P_{\bar{z}}=0$. C parity adds the requirement that $P_{\bar{y}}=P_y$. P and C also impose strong restrictions on the correlation coefficients, $C_{\bar{x}y}=C_{\bar{y}x}=C_{\bar{z}y}=C_{\bar{y}z}=0$ due to P, and $C_{\bar{z}x}=C_{\bar{x}z}$ due to C. However, if we instead begin with a polarized target, as we plan to do in forthcoming measurements [46] of the *depolarization,* these statements will be modified.

Writing out the final-state angular distribution in full using Eqs. (5) and (6), we have

$$W(\cos\theta_{\bar{\Lambda}};\hat{k}_{\bar{p}},\hat{k}_p)=\frac{1}{16\pi^2}\Bigg[1+\alpha P_y\cos\theta_y+\bar{\alpha}P_{\bar{y}}\cos\theta_{\bar{y}}+\alpha\bar{\alpha}\times\sum_{mn}C_{\bar{m}n}\cos\theta_{\bar{m}}\cos\theta_n\Bigg], \tag{8}$$

with $\hat{k}_{\bar{p}}$ and $\hat{k}_p$ being the direction cosines of the outgoing products of the hyperon decays defined in the hyperon rest frame (see Fig. 2). CP invariance requires that $\alpha=-\bar{\alpha}$. The reported value of α is 0.642 ± 0.013 [44].

Using the angular distribution given in Eq. (8), and taking the angular acceptance into account, the polarizations and the spin correlation coefficients obtained by observing N events (i.e., the expectation values) can be expressed [16] in terms of measured values of the direction cosines. For the polarization, averaging Eq. (8) over N measurements yields

$$P_{\bar{y}}=\frac{3}{\bar{\alpha}}\frac{1}{N}\frac{\sum_{k=1}^{N}\zeta_k\cos\theta_{\bar{y}}^k}{\sum_{k=1}^{N}\zeta_k}, \tag{9}$$

while for the correlation coefficient we have

$$C_{\bar{m}n}=\frac{9}{\bar{\alpha}\alpha}\frac{\sum_{k=1}^{N}\zeta_k\cos\theta_{\bar{m}}^k\cos\theta_n^k}{\sum_k\zeta_k}. \tag{10}$$

Here ζ_k is the acceptance correction factor for the detector for each event k. For sufficiently large statistics N the standard deviation in $C_{\bar{m}n}$ is $\sigma_{\bar{m}n}\approx(3/\alpha^2\sqrt{N})$.

Special attention was paid to understanding and correcting for systematic experimental uncertainties (Ziolkowski [1]). For this reason 350 000 Monte Carlo events were generated using isotropic distributions for the reaction products in the center-of-momentum frame and in the rest frames of the $\bar{\Lambda}$ and Λ. This is tantamount to assuming unpolarized hyperon decays. The Monte Carlo sample was analyzed by taking the full detector response into account using the same analysis program as for the real data. We found that the spatial distributions of the decay antiprotons show a loss of

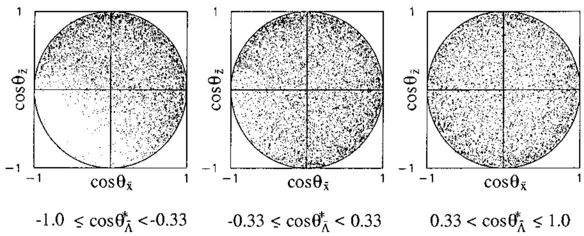

FIG. 3. Projection of the unit vector endpoint onto the $\bar{\Lambda}\Lambda$ production plane for the decay $\bar{p}$ in the $\bar{\Lambda}$ rest frame. The ranges for the cosine of the scattering angle, from left to right, are (-1.0 to -0.33), (-0.33 to 0.33), and (0.33 to 1.0). Fainter regions correspond to inefficiencies.

events (see Fig. 3) in the region where the acceptance is small ($-1.0 \leq \cos\theta_{\bar\Lambda} \leq -0.33$). An equivalent situation occurs for the Λ decay, where an acceptance close to zero is observed for large center-of-mass angles. These losses are explained by the low momenta of the π mesons from the Λ decays, which either were not recorded in the detector system and/or which were rejected by the requirements of the analysis program. In the case where the acceptance factor ζ is zero in Eqs. (9) and (10), the correction is undefined.

In order to overcome these deficiencies, symmetry relations from the CPT theorem were used to generate three additional combinations of kinematic variables that give rise to the same result for the polarization and spin correlation observables. For an arbitrary set of vectors $\hat{k}_{\bar{p}}$ and $\hat{k}_p$, (1) CP invariance allows the interchange of Λ and $\bar{\Lambda}$, a symmetry with respect to the reaction plane; (2) C and P invariance provide a reflection symmetry about the $\bar{y}$ and y axes; and (3) T invariance allows the exchange $\hat{r} \rightarrow -\hat{r}$.

If the measured pattern is replaced event by event by any one of the equivalent transformed patterns, the resulting polarization observables will be unchanged. Therefore the event sample can be ''extended'' to a sample which is 4 times larger and, more importantly, one that allows each event to sample four different parts of the detector. While this greatly improves our understanding of the systematics of the experiment, it of course *does not* enhance the statistical accuracy.

If the acceptance function is uniform, those four events contribute with equal weight to the determination of the spin correlation coefficients. Thus, a smooth, effective acceptance function can be constructed which nowhere drops to zero, and which consequently provides sufficient information to determine the differential spin correlation coefficients $C_{\bar{x}x}, C_{\bar{y}y}, C_{\bar{z}z}$, and $C_{\bar{x}z} = C_{\bar{z}x}$ in the entire center-of-momentum space.

In an additional investigation, an *uncorrelated sample* of events was obtained from the data themselves. To do this, all analyzed $\bar{\Lambda}_n\Lambda_n$ events were ordered according to their production kinematics, and then recombined with nearest neighbors to make hypothetical events, e.g., $\bar{\Lambda}_n\Lambda_{n+1}$. This leads to an event sample which is by construction uncorrelated, allowing us to measure the experimental acceptance function ζ directly. The two methods—the Monte Carlo simulation and the recombination procedure—agree rather well (Ziolkowski [1]). Differences indicate where there are poorly understood detector efficiencies.

V. RESULTS

A. Cross sections

For the 1.642 GeV/c data, approximately 7.2×10^{10} antiprotons were incident on target, giving an integrated luminosity of $\mathcal{L} = 5.1$ nb^{-1}, whereas at 1.918 GeV/c, approximately 5.4×10^{10} incident antiprotons produced a luminosity of $\mathcal{L} = 3.2$ nb^{-1}. At the lower momentum, 43 430 reconstructed events gave a total cross section of $\sigma_{\text{tot}} = 64.1 \pm 0.4 \pm 1.6$ μb, while for the higher momentum 36 977 events led to $\sigma_{\text{tot}} = 88.0 \pm 0.7 \pm 1.9$ μb. The errors quoted are statistical and systematic, respectively. The differential cross sections and polarizations are shown in Figs. 4(a) and 4(c) as a function of center-of-momentum $\cos\theta_{\bar{\Lambda}}$, and in Figs. 4(b) and 4(d) as a function of the *reduced four-momentum transfer squared* t':

$$t' = -t(\theta=0) + m_p^2 + m_\Lambda^2 - \frac{s}{2} + \tfrac{1}{2}\sqrt{(s-4m_p^2)(s-4m_\Lambda^2)}\cos\theta_{\bar{\Lambda}}. \tag{11}$$

The differential cross sections shown in Fig. 4(a) on a logarithmic scale reveal in general the typical behavior for the $\bar{p}p \rightarrow \bar{\Lambda}\Lambda$ reaction as was already observed at lower momenta: A strong forward rise is followed by a rather flat distribution. Such a forward-peaked angular distribution is typical for peripheral processes and for simple absorptive models [13,14] the slope parameter of 9.1 ± 0.5 (GeV/c)$^{-2}$ as extracted from Fig. 4(b)corresponds to an absorption radius of 1.2 ± 0.1 fm. Similar values were deduced for the measurements [48–50] in the threshold region.

At lower incident momentum the slope change from steeply rising to rather flat angular distributions occurs at $t' \simeq -0.2$ (GeV/c)^2. For the rather high momenta discussed here, this change of slope occurs at a more negative value of t', especially for the 1.918 GeV/c data, as can be seen in Fig. 4(b). For the 1.642 GeV/c data the slope change is rather smooth with an indication of a break at $t' = -0.2$ (GeV/c)^2, and a clear turnover to a flat distribution shifted to a value of $t' \simeq -0.35$ (GeV/c)^2. For the 1.918 GeV/c data significant flattening is not observed until $t' \simeq -0.60$ (GeV/c)^2, again with a rather smooth change of the slope towards the steep rise at small scattering angles. In this model a comparison of the two measured cross sections implies a larger absorption radius for the 1.918 GeV/c data.

It is interesting to note the apparent dip in the differential cross section at back angles, especially for the higher-momentum data at 1.918 GeV/c. If real, this observation could indicate new reaction mechanisms and/or nucleon structures. For example, in a meson- or baryon-exchange picture, such features have been interpreted in terms of u-channel baryon exchanges [47]. In quark descriptions, such oscillations can be obtained from models in which spatially extended ''diquarks'' [28] are taken as elementary constituents of baryons in addition to the pointlike quarks of the constituent scattering model. However, a word of caution is necessary since it could be that the backward increase is due very simply to a wrong baryon number identification between $\bar{\Lambda}$ and Λ. A permutation in 4% of the cases could produce the backward increase that is observed. Although we

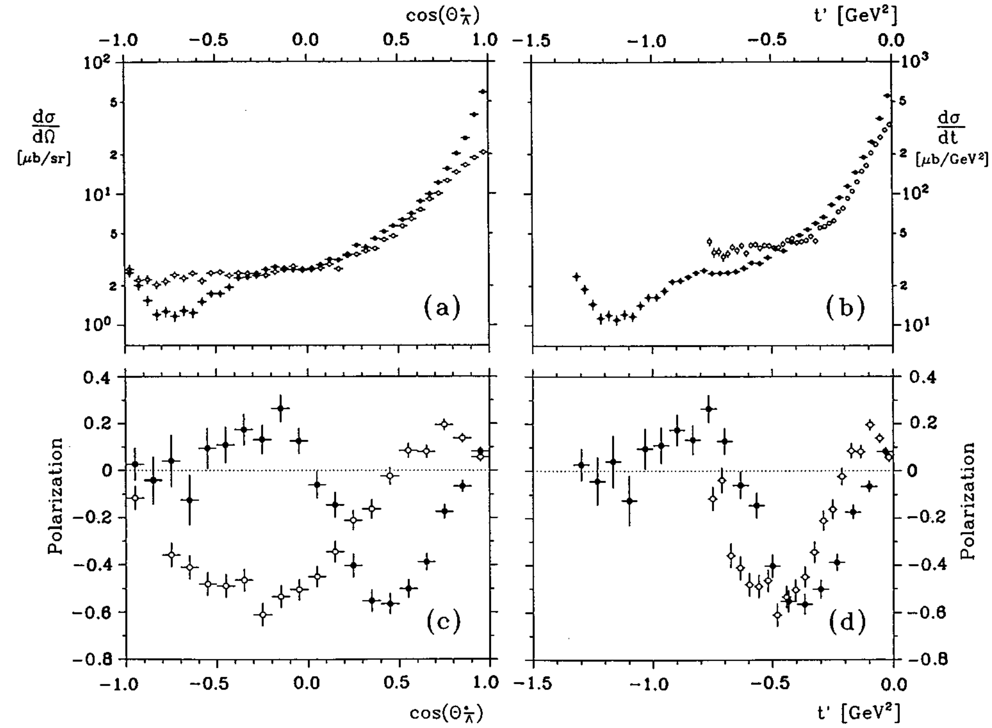

FIG. 4. Cross sections (upper panels) and polarizations (lower panels) from this experiment. Open circles: data at 1.642 GeV/c. Solid circles: data at 1.918 GeV/c. The left hand panels (a) and (c) show the data as a function of $\cos\theta$. The right hand panels (b) and (d) show it as a function of reduced four momentum transfer squared, t'.

are confident of our analysis, we do not wish to place strong emphasis on the physics interpretation given the small margin for error.

Regarding the reaction dynamics, it is obvious that at higher beam momentum contributions from higher partial waves will be observed. This is seen in the slope of the differential cross section as well as by the comparison of the Legendre polynomial coefficients, extracted to fit the experimental data and compared to each other in Table I. It should be noted that the appearance of the coefficient A_8 is closely linked to the back-angle structure discussed in the above paragraph.

B. Polarization

Because the antihyperon-hyperon pair is produced in a strong interaction process, parity conservation allows only the polarization component perpendicular to the reaction plane (i.e., the $\hat{y}$ direction) to be nonzero (assuming an unpolarized initial state). In addition, because the reaction plane is undefined at $\theta_{\bar{\Lambda}}=0$ and π, the polarization must vanish there. In Fig. 4 the polarizations averaged over $\bar{\Lambda}$ and Λ are shown both as a function of $\cos\theta_{\bar{\Lambda}}$ [Fig. 4(c)] and as a function of the reduced square of the momentum transfer t' [Fig. 4(d)]. The open circles are the data at 1.642 GeV/c; the solid circles are the data at 1.918 GeV/c. The 1.642 GeV/c data exhibit polarization characteristics similar to those observed previously at lower beam momenta [2–4]: $P_{\bar{y}}>0$ over the range from $t'=0$ to $t'=-0.2$ (GeV/c)^2; it crosses zero at that point and remains negative with decreasing t' until the minimum value of t' is reached. The 1.918 GeV/c data illustrate somewhat different behavior in that the initial sign change occurs at a much smaller value of t'[-0.08 (GeV/c)^2] (Ziolkowski [1]). And while at 1.642 GeV/c only one zero crossing is observed, the 1.918 GeV/c data show a second one at 90° center-of-momentum angle or $t'=-0.65$ (GeV/c)^2. This value is rather close to the point at which the shape change of the differential cross section occurs. At larger reduced squared momentum transfers $|t'|>1.1$ (GeV/c)^2 (equivalent to $-0.7<\cos\theta_{\bar{\Lambda}}<-1.0$) the polarization is consistent with zero.

TABLE I. Coefficients resulting from Legendre polynomial fits to the $\bar{p}p\to\bar{\Lambda}\Lambda$ differential cross sections obtained at 1.642 and 1.918 GeV/c.

Coefficient	1.642 GeV/c Value ± error	1.918 GeV/c Value ± error
A_0	5.097 ± 0.035	7.033 ± 0.053
A_1/A_0	1.238 ± 0.018	1.775 ± 0.023
A_2/A_0	1.195 ± 0.022	1.919 ± 0.031
A_3/A_0	0.738 ± 0.024	1.659 ± 0.035
A_4/A_0	0.028 ± 0.027	1.374 ± 0.037
A_5/A_0	−0.041 ± 0.029	0.826 ± 0.036
A_6/A_0	−0.065 ± 0.031	0.622 ± 0.035
A_7/A_0	−0.094 ± 0.029	0.337 ± 0.029
A_8/A_0	−0.009 ± 0.028	0.118 ± 0.023

C. Spin correlations and singlet fraction

In Fig. 5(a) the differential spin correlation coefficient distributions are shown. The errors are dominated by statistics and thus they increase at large angles where the differential cross section is small. As for the case of the polarization, the reaction plane is undefined at $\cos\theta_{\bar{\Lambda}}=\pm1$, and so it is expected that $C_{\bar{x}\bar{z}}=C_{\bar{z}\bar{x}}=0$ and $C_{\bar{x}\bar{x}}=-C_{\bar{y}\bar{y}}$ at those angles. The data in Fig. 5(a) are consistent with these statements.

The coefficient $C_{\bar{y}\bar{y}}$ is positive for angles $\theta_{\bar{\Lambda}}\leq 90°$ with a maximum value close to unity at $\cos\theta_{\bar{\Lambda}}\simeq 0.3$. While the

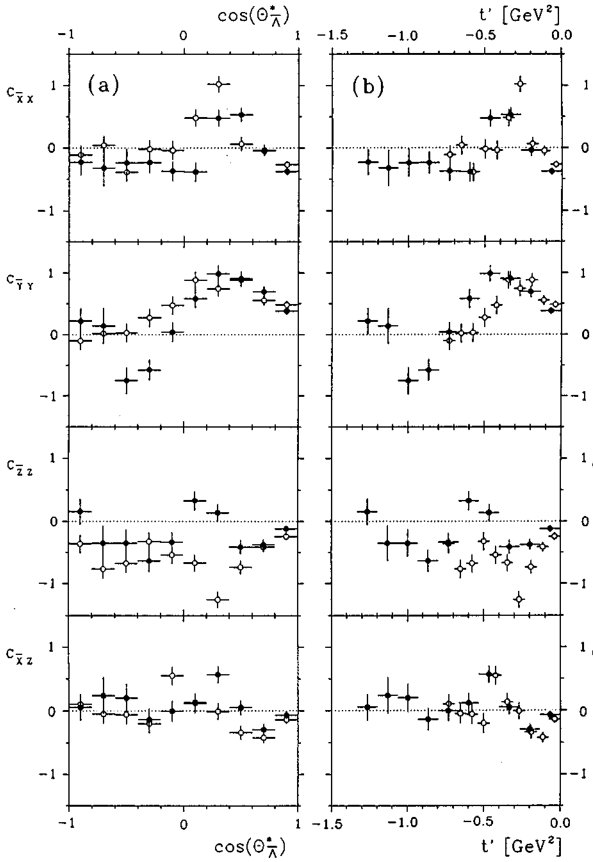

FIG. 5. Spin correlations. Open circles: data at 1.642 GeV/c. Solid circles: data at 1.918 GeV/c. Panel (a) shows the data as a function of $\cos\theta$. Panel (b) shows it as a function of reduced four-momentum transfer squared t'.

1.918 GeV/c data show negative spin correlation values for scattering angles $\theta_{\bar{\Lambda}} \leq 90°$, the values for the 1.642 GeV/c spin correlations decrease to values around zero. Less pronounced structures are observed for the other correlation coefficients. Figure 5(b) shows the spin correlations as a function of the reduced momentum transfer t'.

The three diagonal elements of the spin correlation matrix are combined to form the singlet fraction

$$S_F = \tfrac{1}{4}(1 - \langle \vec{\sigma}_{\bar{\Lambda}} \cdot \vec{\sigma}_{\Lambda} \rangle) = \tfrac{1}{4}(1 + C_{\bar{x}x} - C_{\bar{y}y} + C_{\bar{z}z}), \quad (12)$$

where the coordinate system is the one as given in Fig. 2. The expected value for S_F when there is no spin correlation is 1/4. This is determined by simple statistical weighting of the three triplet and one singlet magnetic substates.

The differential singlet fraction is shown in Fig. 6. Averaging over angle yields $\langle S_F \rangle = -0.003 \pm 0.015$ for the 1.642 GeV/c data and $\langle S_F \rangle = 0.058 \pm 0.016$ for the 1.918 GeV/c data.

The data at the lower momentum lead to $\langle S_F \rangle$ values which are consistent with zero; this indicates a pure triplet production of the $\bar{s}s$ strange quark pair. In the 1.918 GeV/c data a slightly positive value is observed with 3.5σ confidence interval. This measurement is the first one with high statistics above the $\bar{p}p \to \bar{\Sigma}^0 \Sigma^0$ thresholds and could reflect a coupling to these channels.

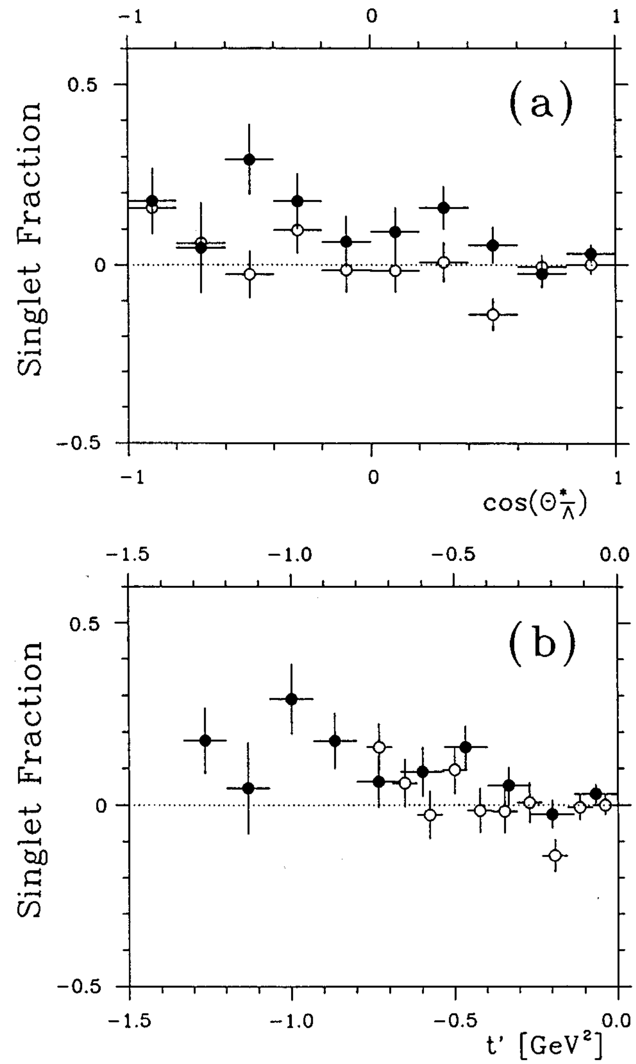

FIG. 6. Singlet fractions. Open circles: data at 1.642 GeV/c. Solid circles: data at 1.918 GeV/c. Panel (a) shows the data as a function of $\cos\theta$. Panel (b) shows it as a function of reduced four-momentum transfer squared t'. The unweighted statistical value would be 1/4.

It will be interesting to see whether the observed nonzero value for $\langle S_F \rangle$ at 1.918 GeV/c is confirmed by additional measurements taken by the PS185 collaboration around the $\bar{\Sigma}^0 \Sigma^0$ and $\bar{\Sigma}^{\pm} \Sigma^{\mp}$ thresholds. The trend of the data as the absolute value of the momentum transfer increases seems to be away from pure triplet production, and possibly toward the statistically expected mixture.

D. Test for *CP* violation

CP violation has only been observed in neutral kaon systems. Though several models can account [51–55] for *CP* violation, the effects seen in the current weak interaction data are still not adequate to distinguish among these models. As described in [7] we evaluate the asymmetry parameter A, defined as

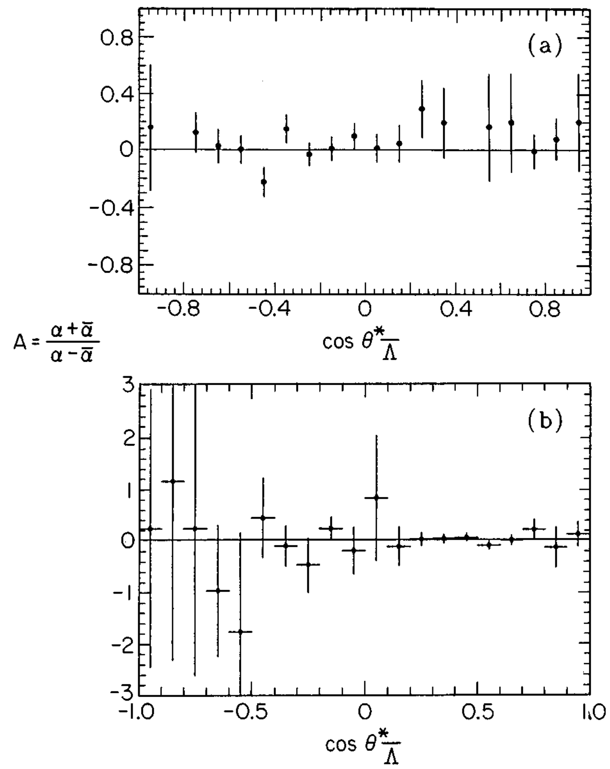

FIG. 7. Angular distributions of the ratio $A=\langle(\alpha+\overline{\alpha})\rangle/\langle(\alpha-\overline{\alpha})\rangle$. The top panel shows data at 1.642 GeV/c and the bottom one shows data at 1.918 GeV/c.

$$A=\frac{\alpha+\overline{\alpha}}{\alpha-\overline{\alpha}} \tag{13}$$

using the present data. Here α and $\overline{\alpha}$ are the decay parameters for the nonleptonic Λ and $\overline{\Lambda}$ weak decays. A nonzero value of A would indicate a direct CP violation. Owing to the weak decay $\overline{\Lambda}\to\overline{p}\pi^+$ the angular distribution of the $\overline{p}$ from the $\overline{\Lambda}$ decay is

$$I(\theta_{\overline{p}})=I_0(1+\overline{\alpha}P_{\overline{y}}\cos\theta_{\overline{p}}), \tag{14}$$

with $\theta_{\overline{p}}$ being defined in the $\overline{\Lambda}$ rest frame between the decay $\overline{p}$ direction and the $\overline{y}$ axis (see Fig. 2). Adapting the ''method of weighted sums'' [56] for a sample of N decaying $\overline{\Lambda}$ particles leads to the expression

$$\overline{\alpha}P_{\overline{y}}=\frac{\sum_{k=1}^{N}\cos\theta_{\overline{p}}^{k}}{\sum_{k=1}^{N}\cos^2\theta_{\overline{p}}^{k}}. \tag{15}$$

Invariance of the strong force under C parity requires $P_{\overline{y}}(\cos\theta)=P_y(\cos\theta)$, allowing a determination of A from the experimental data using Eq. (13).

In Fig. 7 the differential values of A are presented for both momenta, the upper data from 1.642 GeV/c and the lower from 1.918 GeV/c. Large error bars (or missing values) arise due to small values of the respective polarizations

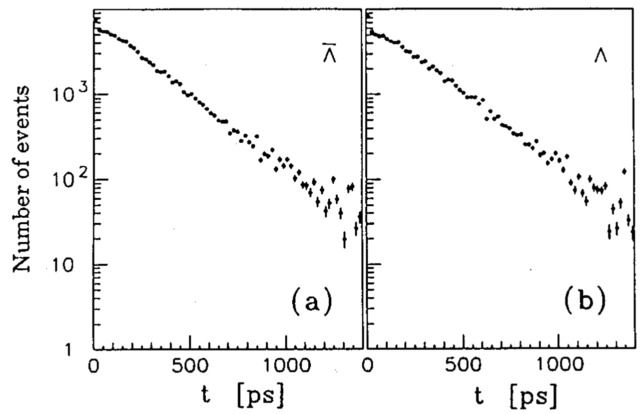

FIG. 8. Lifetime distributions of $\overline{\Lambda}$ (left) and Λ (right), corrected via Monte Carlo simulations.

(see Fig. 4). The data seem to be consistent with zero at both incident $\overline{p}$ momenta. Our evaluation yields mean values of

$$\langle A(1.642\ \text{GeV}/c)\rangle=0.026\pm0.030,$$

$$\langle A(1.918\ \text{GeV}/c)\rangle=0.010\pm0.037. \tag{16}$$

Summing the present results with earlier published measurements of the PS185 experiment (totaling 95 832 events) leads to an asymmetry parameter of $\langle A\rangle=0.013\pm0.022$. While this result represents the best measurement to date of CP violation outside the neutral kaon system, it is still an order of magnitude away from providing a stringent test of theoretical models. However, there remains still a considerably larger set of PS185 data that have not been included here, which when analyzed will reduce the error on the CP-violation limit further.

E. Test of the CPT theorem

According to quantum field theory, the CPT invariance theorem applies very generally to particle interactions. CPT invariance requires equal rest masses and lifetimes for a particle and its antiparticle. The decay length of the hyperons is proportional to the product of momentum and lifetime τ. The lifetime distribution follows a simple exponential law:

$$\frac{dN}{dt}=N_0e^{-t/\tau}. \tag{17}$$

Thus with the present experimental setup the lifetime distributions of both $\overline{\Lambda}$ and Λ could be extracted for a given momentum in the same experiment. Figure 8 shows the results for the 1.642 GeV/c data (Fischer [1]). The lifetime values we extract are

$$\tau_{\overline{\Lambda}}=258.4\pm4.7\pm5.3\ \text{ps},$$

$$\tau_{\Lambda}=265.2\pm4.3\pm5.3\ \text{ps}, \tag{18}$$

with statistical and systematical uncertainties, respectively, shown in order. Using extensive Monte Carlo simulations these results have been corrected for the specific features of our detector.

In order to reduce the Monte Carlo corrections on the lifetime measurements when comparing the $\bar{\Lambda}$ and Λ lifetimes, we applied momentum- and decay-point-dependent cuts. Thus, the detector acceptance is assumed to be equal in certain regions for the hyperon decay products. This special sampling leads to a ratio

$$R=\frac{\tau-\overline{\tau}}{(\tau+\overline{\tau})/2}=(-1.8\pm 6.6\pm 5.6)\times 10^{-3}. \tag{19}$$

Details are presented by Fischer [1]. This evaluation is an order-of-magnitude more precise than the only other measurement [57] reported to date.

VI. DISCUSSION

Differential cross sections, polarizations, and spin correlations have been presented at incident antiproton momenta of 1.642 and 1.918 GeV/c for the reaction $\bar{p}p\to\bar{\Lambda}\Lambda\to\bar{p}\pi^{+}p\pi^{-}$. There are about 40 000 reconstructed events in each sample.

The angular distributions shown in Fig. 4 indicate that the slope of the data at small angles is significantly steeper for the 1.918 GeV/c data than for the 1.642 GeV/c data. This would seem to indicate a larger interaction range at the higher momentum. In both cases, as in all previous measurements of PS185, the forward peaking dissolves at larger angles into an almost flat, featureless distribution.

The differential polarizations at the two momenta exhibit structures that are distinct from each other, the higher-momentum data displaying an additional node. As suggested from the differential cross sections, higher partial wave contributions and their coherent interference are probably responsible for the change of the pattern from that observed at lower beam momenta. The influence of a coupled-channel effect on the structure should be further investigated in high-statistics measurements below and above the $\bar{p}p\to\bar{\Sigma}^{\pm}\Sigma^{\pm}$ channels.

The weighted mean of all the measured singlet fraction data from the PS185 experiment published to date, $\langle S_F\rangle=0.007\pm 0.009$, is consistent with zero. This indicates that $\bar{\Lambda}\Lambda$ production is occurring in a pure triplet state. However, at 1.918 GeV/c a small but positive value of $\langle S_F\rangle=0.058\pm 0.016$ is observed, which may indicate that at higher absolute value of the momentum transfer the $\bar{\Lambda}\Lambda$ production is tending toward the value expected based on simple spin statistics.

In the naive quark model the lowest-order process for the $\bar{p}p\to\bar{\Lambda}\Lambda$ reaction is the annihilation of a $\bar{u}u$ quark pair followed by the production of an $\bar{s}s$ quark pair. In these models the other quark pairs in the participating baryons are regarded as spin and isospin $S=I=0$ spectators that do not influence the reaction dynamics. Because of the vanishing of the experimentally measured singlet fraction, most of the quark model applications calculate the s-channel vector ($^3S_1$) and/or scalar ($^3P_0$) exchange only, and result necessarily in $S_F=0$ triplet $\bar{s}s$ pair production. Following Alberg *et al.* [24] a pseudoscalar s-channel exchange could proceed via the exchange of an intermediate η or η', since these mesons possess strong strange–antistrange-quark flavor content. Then the pseudoscalar contribution is weak due to small coupling constants and high spin multiplicities. Qualitatively, the present small value of $\langle S_F\rangle$ is in agreement with these considerations.

In a t-channel meson exchange picture [16,18,19] interferences between the K, K^*, and K^{**} meson exchanges are needed in order to enhance the strong tensor component and to cancel partially the central potential components. Calculations result in a singlet fraction $\langle S_F\rangle$ of only a few percent, whereas a decrease of $K-K^*$ interference would lead to an increasing S_F contribution. According to [41] a large tensor ($\ell-\ell'=2$) transition in $\bar{p}p\to\bar{\Lambda}\Lambda$ is expected due to the strong tensor force of the $K-K^*$ exchange. This is one reason why the PS185 collaboration will measure the depolarization in the $\bar{p}p\to\bar{\Lambda}\Lambda$ reaction employing a frozen spin target [58].

As expected with the present accuracy, CP-violation effects in the weak interaction have not been observed in either experiment presented here. Summing the present results with earlier published measurements of PS185 (totalling 95 832 events) leads to an asymmetry parameter of $\langle A\rangle=0.013\pm 0.022$. This value is essentially consistent with zero. However, the PS185 experiment is still about an order of magnitude away from providing enough statistics to test present theoretical models. Similarly, for the CPT test, the lifetimes of both $\bar{\Lambda}$ and Λ are found to be identical at the 10^{-3} level.

In the near future, the PS185 Collaboration will publish data for the $\bar{\Lambda}\Lambda$ channel at several other incident momenta and for other hyperon reaction channels. We expect that these data will extend our general understanding of this interesting set of reactions.

ACKNOWLEDGMENTS

The members of the PS185 Collaboration thank the LEAR accelerator team for the excellent preparation of the antiproton beam. We would also like to thank Professor Mary Alberg for a very helpful critique of our manuscript. We also gratefully acknowledge financial and material support from the Austrian Science Foundation, the German Bundesministerium für Forschung und Technologie, the Swedish Natural Science Research Council, the U.S. Department of Energy (Grant No. DE-FG02-87ER40315), and the U.S. National Science Foundation (Grant No. PHY-94-20787). This work is based on the Ph.D. theses of H. Fischer and M. Ziolkowski, submitted to the Universities of Freiburg and Cracow, respectively, in partial fulfillment of the requirements for the Ph.D. degree.

[1] R. Bröders, Ph.D. thesis, Jülich, 1995; H. Dennert, Ph.D. thesis, Erlangen-Nürnberg (in preparation); W. Dutty, Ph.D. thesis, Freiburg, 1988; H. Fischer, Ph.D. thesis, Freiburg, 1992; R. von Frankenberg, Ph.D. thesis, Erlangen-Nürnberg, 1989; R. Geyer, Ph.D. thesis, Erlangen-Nürnberg, 1993; J. Hauffe, Ph.D. thesis, Erlangen-Nürnberg (in preparation); T. Jones, Ph.D. thesis, Illinois, Urbana-Champaign (in preparation); R.-A. Kraft, Ph.D. thesis, Erlangen, 1994; C. Maher, Ph.D. thesis, Carnegie Mellon, 1986; S. Ohlssen, Ph.D. thesis, Uppsala, 1990; K. Sachs, Ph.D. thesis, Jülich (in preparation); H. Schlederman, Ph.D. thesis, Freiburg, 1989; T. Sefzick, Ph.D. thesis, Jülich, 1991; G. Sehl, Ph.D. thesis, Jülich, 1989; J. Seydoux, Ph.D. thesis, Carnegie Mellon, 1990; F. Stinzing, Ph.D. thesis, Erlangen-Nürnberg, 1991; R. Tayloe, Ph.D. thesis, Illinois, Urbana-Champaign 1995; R. Todenhagen, Ph.D. thesis, Freiburg, 1995; M. Ziolkowski, Ph.D. thesis, Cracow and Jülich, 1993.
[2] P. Barnes *et al.*, Phys. Lett. B **189**, 249 (1987).
[3] P. Barnes *et al.*, Phys. Lett. B **229**, 432 (1989).
[4] P. Barnes *et al.*, Nucl. Phys. **A526**, 575 (1991).
[5] P. Barnes *et al.*, Phys. Lett. B **331**, 203 (1994).
[6] P. Barnes *et al.*, Phys. Lett. B **246**, 273 (1990).
[7] P. Barnes *et al.*, Phys. Lett. B **199**, 147 (1987).
[8] B. Jayet *et al.*, Nuovo Cimento A **45**, 371 (1978).
[9] B. Y. Oh *et al.*, Nucl. Phys. **B51**, 57 (1973).
[10] S. M. Jacobs *et al.*, Phys. Rev. D **17**, 1187 (1978).
[11] H. W. Atherton *et al.*, Nucl. Phys. **B69**, 1 (1974).
[12] H. Becker *et al.*, Nucl. Phys. **B141**, 48 (1978).
[13] See D. Perkins, *Introduction to High Energy Physics*, 3rd ed. (Addison-Wesley, Reading, MA, 1987).
[14] M. Perl, *High Energy Hadron Physics* (Wiley, New York, 1974).
[15] J. Niskanen, Helsinki Report No. HU-TFT-85-28, 1985.
[16] F. Tabakin and R. A. Eisenstein, Phys. Rev. C **31**, 1857 (1985).
[17] A. Green and J. Niskanen, Prog. Part. Nucl. Phys. **18**, 93 (1987).
[18] M. Kohno and W. Weise, Phys. Lett. B **179**, 15 (1986); **206**, 584 (1988); Nucl. Phys. **A479**, 433c (1988).
[19] W. Weise, Nucl. Phys. **A558**, 219c (1993).
[20] P. LaFrance and B. Loiseau, Nucl. Phys. **A528**, 557 (1991); P. LaFrance, B. Loiseau, and R. Vinh Mau, Phys. Lett. B **214**, 317 (1988).
[21] Y. Lu and M. Locher, Z. Phys. A **346**, 143 (1993).
[22] M. Alberg, E. Henley, and L. Wilets, Z. Phys. A **331**, 207 (1988).
[23] M. Alberg, E. Henley, and L. Wilets, Phys. Rev. C **38**, 1506 (1988).
[24] M. Alberg, E. Henley, and W. Weise, Phys. Lett. B **255**, 498 (1991).
[25] M. Alberg, E. M. Henley, L. Wilets, and P. D. Kunz, Nucl. Phys. **A560**, 365 (1993); in Proceedings of the Second Biennial Workshop on Nucleon-Antinucleon Physics, edited by Yu. Kalashnikova, L. Kondratyuk, A. Kudryavtsev, and N. Smorodinskaya, Moscow, 1993 (Yad. Fiz. **57**, 1678 (1994) [Phys. At. Nucl. **57**, 1608 (1994)].
[26] H. Genz and S. Tatur, Phys. Rev. D **30**, 63 (1984).
[27] G. Brix, H. Genz, and S. Tatur, Phys. Rev. D **39**, 2054 (1989).
[28] P. Kroll, B. Quadder, and W. Schweiger, Nucl. Phys. **B316**, 373 (1989).
[29] H. Genz, M. Nowakowski, and D. Woitschitzky, Phys. Lett. B **260**, 179 (1991).
[30] S. Furui and A. Faessler, Nucl. Phys. **A468**, 669 (1987).
[31] M. Burkhardt and M. Dillig, Phys. Rev. C **37**, 1362 (1988).
[32] J. Vandermeulen, Z. Phys. C **37**, 563 (1988).
[33] H. Rubinstein and H. Snellman, Phys. Lett. **165B**, 187 (1985).
[34] F. Tabakin, R. A. Eisenstein, and Y. Lu, Phys. Rev. C **44**, 1749 (1991).
[35] A. Kudriyavtsev and V. Samoilov, Mod. Phys. Lett. A **4**, 721 (1989).
[36] A. Schneider-Neureither *et al.*, Z. Phys. A **344**, 317 (1993).
[37] O. Dalkarov, K. Protasov, and I. Shapiro, Int. J. Mod. Phys. A **5**, 2155 (1990).
[38] I. Shapiro, Nucl. Phys. **A478**, 665c (1988).
[39] J. Carbonell, K. Protasov, and O. Dalkarov, Nucl. Phys. **A558**, 353c (1993).
[40] R. Timmermans, T. Rijken, and J. de Swart, Nucl. Phys. **A479**, 383c (1988); Phys. Rev. D **45**, 2288 (1992); Phys. Lett. B **257**, 227 (1991).
[41] J. Haidenbauer *et al.*, Phys. Rev. C **45**, 931 (1992); **46**, 2158 (1992); **46**, 2516 (1992).
[42] Y. Lu and F. Tabakin (unpublished).
[43] L. Durand and J. Sandweiss, Phys. Rev. **135**, B540 (1964).
[44] Particle Data Group, Phys. Lett. B **239**, 1 (1990).
[45] M. Jacob and G. C. Wick, Ann. Phys. (N.Y.) **7**, 404 (1959).
[46] PS185 Collaboration, B. Bassalleck *et al.*, Report No. CERN-SPSLC/95-13, 1995.
[47] V. Barger and D. Cline, *Phenomenological Theories of High Energy Scattering* (Benjamin, New York, 1969).
[48] H. Schmitt *et al.*, in Proceedings of the IXth European Symposium on Proton-Antiproton Interactions and Fundamental Symmetries, Mainz, Germany, 1988, edited by K. Kleinknecht and E. Klempt [Nucl. Phys. **B8**, 162 (1989)].
[49] T. Johansson, in Proceedings of the Second Conference on Particle Production near Threshold, edited by C. Ekstrom, B. Hoistad, A. Johansson, and S. Kullander [Phys. Scr. Reprint Series No. 21, 102 (1993)].
[50] R. A. Eisenstein, in Proceedings of the Second Biennial Workshop on Nucleon–Antinucleon Physics, edited by Yu. Kalashnikova, L Kondratyuk, A. Kudryavtsev, and N. Smorodinskaya, Moscow, 1993 (Yad. Fiz. **57**, 1751 (1994) [Phys. At. Nucl. **57**, 1680 (1994)].
[51] L. Wolfenstein, Phys. Rev. Lett **13**, 562 (1964).
[52] S. Weinberg, Phys. Rev. Lett **37**, 657 (1976).
[53] R.N. Mohapatra *et al.*, Phys. Rev. D **11**, 566 (1975).
[54] L.L. Chau, Phys. Rep. **95**, 1 (1983).
[55] L. Wolfenstein, Annu. Rev. Nucl. Part. Sci. **36**, 137 (1986).
[56] D. Besset *et al.*, Nucl. Instrum. Methods **166**, 515 (1979).
[57] J. Badier *et al.*, Phys. Lett. **25B**, 152 (1967).
[58] H. Dutz *et al.*, Nucl. Instrum. Methods A **340**, 272 (1994); B. Bassalleck *et al.*, Proposal P287, Report No. CERN/SPSLC 95-13 (accepted as PS185-3).